Inorganic Chemistry

Article

pubs.acs.org/IC

# Europium(III) Tetrakis(β-diketonate) Complex as an Ionic Liquid: A Calorimetric and Spectroscopic Study

Cláudia C. L. Pereira,*[,‡] Sofia Dias,[†] Isabel Coutinho,[†] J. P. Leal,[‡,§] Luís C. Branco,[†] and César A. T. Laia*[,†]

[†]Chemistry Department, REQUIMTE, Faculdade de Ciências e Tecnologia, 2829-516 Caparica, Portugal

[‡]Unidade de Ciências Químicas e Radiofarmacêuticas, Instituto Superior Técnico, Instituto Tecnológico e Nuclear, Estrada Nacional 10, 2686-953 Sacavém, Portugal

[§]Centro de Química e Bioquímica, Faculdade de Ciências, Universidade de Lisboa, Campo Grande, 1749-016 Lisboa, Portugal

Supporting Information

**ABSTRACT:** An intrinsic photoluminescent ionic liquid based on europium(III) tetrakis(β-diketonate) complex with a tetraalkylphosphonium as counterion was synthesized. Calorimetric measurements showed a melting point at 63 °C, which allows the ionic liquid classification. When cooling the material from the liquid state, metastable supercooled ionic liquid is obtained, as seen from NMR spectroscopy as well. Eu(III) photoluminescence is clearly observed while the absorption spectra of the ligand is dominant, showing the antenna effect. This was confirmed with submicrosecond time scale luminescence spectroscopy, where a rise of Eu(III) emission is observed with the correspondent decay of the ligand excited state. Temperature effects in the photoluminescence are also shown, being prominent above the melting point where the intensity decreases with Arrhenius behavior. Eu(III) luminescence decays also show features characteristic of energy migration between homologue Eu(III) species. Solvent effects were also studied by NMR and Luminescence spectroscopies, highlighting that the nucleophilicity of organic solvents such as *n*-alcohols leads to a coordination with Eu(III), which ultimately compromises the stability of the complex.

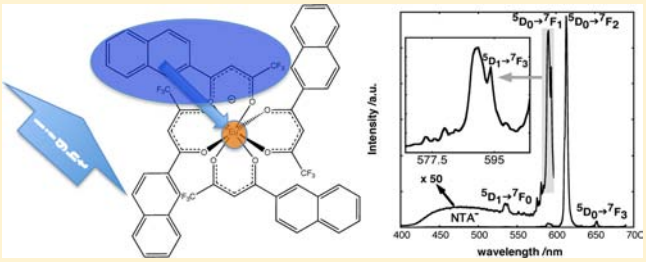


## INTRODUCTION

Trivalent lanthanide complexes ($Ln^{III}$) are of great interest because of a wide range of applications such as luminescent materials,[1,2] laser materials,[3] luminescent labels,[4] fluorescent lamps, and cathode ray-tubes.[5] Europium(III) and β-diketonate ligands have been extensively studied in the past four decades because of their ability to function as light conversion molecular devices such as OLEDs (organic light-emitting diodes).[6] Generally, for lanthanides, the trivalent cations ($Ln^{III}$) display absorption and emission bands that correspond to Laporte forbidden f-f transitions, and therefore direct excitation of $Ln^{3+}$ is very inefficient. This is overcome by using a strongly absorbing chromophore (organic ligand) that after excitation transfers the energy to the Ln(III) ion, which then emits. β-Ketonate ligands are one of the most important "antennas" with strong absorption within a large wavelength range for its $\pi-\pi^*$ transitions.[7−10] Europium(III) β-diketonates have been intensively studied either as tris(β-betadiketonate) complexes containing other ligands such as nitrogen compounds (1,10-phenanthroline, 2,2′-bipyridine, 4,4′-disubstituted-2,2′-bipyridines, 1,4-diaza-1,3-butadienes, and 2,2′,6′,6″-terpyridine)[11] or as tetrakis complexes with all coordination positions filled with 4 betadiketonate units and charge neutrality provided by a selected organic cation ([Cation][Ln(β-betadiketonate)$_4$].[12] For naphthoyltrifluoroacetone (NTA) complexes of Gd(III) and Eu(III) different adequate counterions were used such as tetrabutylammonium, $[NBu_4]^+$, 1-butyl-3-methylimidazolim, $[C_4mim]^+$, and 1-butyl-3-methylpyridinium, $[C_4mpyr]^+$, and their photoluminescence properties studied.[2] Regarding the thermal behavior for Eu(III) complexes, Differential Scanning Calorimetry (DSC) and Thermogravimetry Analysis (TGA) indicated melting points of 197, 150, and 200 °C, respectively for $[NBu_4]^+$, $[C_4mim]^+$, and $[C_4mpyr]^+$ compounds.

Metal-containing ionic liquids combine the best of two worlds, namely, the properties of ionic liquids, negligible vapor pressures, good thermal stabilities, considerable electric conductivities, and wide electrochemical range, and those of the metal ion that include magnetic, photophysical, optical or catalytic applications.[13] Two terbium β-diketonate based ionic liquids, with melting point of 116.2 and 111.4 °C, respectively for $[C_4mim][Tb(hfacac)_4]$ and $[C_4mpyr][Tb(hfacac)_4]$, (hfacac = hexafluoracetylacetone), showed typical luminescence in the green region, characteristic of Tb(III) compounds.[14] Other lanthanide tetrakis beta-diketonate complexes were also studied in ionic liquids as dopants, providing, for example, ways to

**Received:** October 19, 2012
**Published:** March 11, 2013

   dx.doi.org/10.1021/ic3023024 | *Inorg. Chem.* 2013, 52, 3755−3764

study ionic liquids confined on silica networks and showing the feasibility of developing luminescent ionic liquids based on lanthanides.[15−19] In the present work a new ionic liquid was synthesized by using a tetraalkylphosphonium $[P_{6,6,6,14}]^+$ as counterion of a europium(III) tetrakis(β-diketonate) complex (Scheme 1). The photoluminescence and thermochemical properties of the complex were investigated in detail for this compound.

**Scheme 1.** $[P_{6,6,6,14}][Eu(NTA)_4]$ **Ionic Liquid**

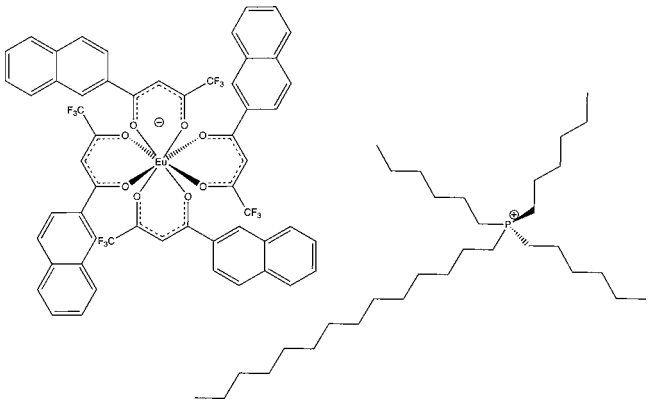

## EXPERIMENTAL SECTION

**Reagents.** The following reagents and solvents were used without further purification: europium chloride hexahydrate (Alfa Aesar, 99.9%), HNTA (Aldrich), $[P_{6,6,6,14}]Cl$ (Cytec), absolute ethanol (Aldrich, p.a.). Spectroscopic grade organic solvents were purchased from Sigma-Aldrich. Different deuterated solvents were purchased from Cambridge Isotopes.

**Synthesis of $[P_{6,6,6,14}][Eu(NTA)_4]$.** A solution of NaOH (1.91 mL, 1 M) was added to a solution of HNTA (0.51 g, 1.91 mmol) in 20 mL of ethanol at room temperature. 140 mg (0.382 mmol) of $EuCl_3{\cdot}6H_2O$ were then added very slowly, and the solution was stirred for 4 h at 50 °C. After cooling, a solution of 198.2 mg (0.382 mmol) of $[P_{6,6,6,14}]Cl$ in ethanol was added, and the mixture stirred for another 2 h at room temperature. The solvent was removed under reduced pressure, and the compound was obtained as a yellow oil after extraction with dichloromethane. This product becomes solid after a few hours. Yield: 0.62 g (95%)

Selected IR ($cm^{-1}$) 684 (m, C═C), 790 (s, C═C), 1133 (s, C−F), 1299 (vs, C−P), 1465 (s, C−C), 1530 (s, C−C), 1570 (s, C−C), 1600 (s, C−C), 1614 (vs, C═O), 2860 (m, $CH_3$), 2926 (m, $CH_3$), 3050 (w, C═CH). (w - weak, m - medium, s - strong, vs - very strong). $^1H$ NMR (400 MHz; r.t., $CDCl_3$, ppm): 7.39−8.04 (m, 28H, naphthyl-H), 6.88 (br s, 4H, CH of β-diketone), 5.08 (m, 8H, P-$CH_2$), 2.80 (m, 8H, P-$CH_2$-$CH_2$), 2.20 (m, 8H, P-$CH_2$-$CH_2$-$CH_2$), 1.60 (m, 8H, P-$CH_2$-$CH_2$-$CH_2$-$(CH_2)_n$-$CH_2$-$CH_3$), 1.18−1.21 (m, 24H, P-$CH_2$-$CH_2$-$CH_2$-$(CH_2)_n$-$CH_2$-$CH_3$), 0.88 (m,12H, P-$CH_2$-$CH_2$-$CH_2$-$(CH_2)_n$-$CH_2$-$CH_3$). $^{13}C$ NMR (100 MHz; r.t., $CDCl_3$, ppm), 135.9, 129.6, 128.9, 127.8, 126.7, 125.4, 122.7, 77.3, 76.9, 76.7, 31.9, 31.4, 31.1, 29.6, 29.3, 22.9, 22.6, 22.4, 21.3, 20.8, 13.9. MS (ESI-) (*m*/*z*): 1212 ($[^{151}Eu(NTA)_4^-]$), 1213.9 ($[^{153}Eu(NTA)_4^-]$); MS (ESI+) (*m*/*z*): 483.4 ($PC_{32}H_{68}^+$) (see Supporting Information for ESI and $^1H$ NMR spectra).

**Equipment and Measurements.** *Electrospray Ionization Mass Spectrometry (ESI-MS).* ESI-MS was performed using a Bruker HCT quadrupole ion trap mass spectrometer. Sample solutions approximately $10^{-5}$ M in acetonitrile were introduced to the ESI source via a syringe pump at a flow rate of 150 mL $min^{-1}$. The heated capillary temperature was set to 250 °C and the cover gas ($N_2$) to a flow rate of 2 L $min^{-1}$. Both positive and negative modes were detected to see the existing cations and anions.

*Magnetic Resonance (MR).* MR spectra for the nuclei $^1H$, $^{13}C$, $^{19}F$, and $^{31}P$ were collected using an NMR spectrometer Bruker Avanced 400 equipped with a BDO multinuclear probe. Data was obtained in 5 mm standard NMR sample tubes with a coaxial capillary containing $D_2O$ for locking when necessary. Phase transitions of $[Eu(III)(NTA)_4](P_{6,6,6,14})]$ were monitored when subjecting the solid sample to successive 5 °C heating steps up to 90 °C followed by similar stepwise cooling to room temperature (25 °C). $^1H$, $^1H$-$^{13}C$ correlation, $^{31}P$ and $^{19}F$ NMR spectral data were acquired after allowing the temperature to stabilize for at least 10 minutes. Temperatures quoted were those presented in the spectrometer temperature control unit. Standard 1D and 2D-pulse programs were used; $^{19}F$-$^{19}F$ EXSY experiments were performed with a delay time of 500 ms.

*Differential Scanning Calorimetry.* DSC was performed using the equipment from Setaram, model DSC 131. The temperature range was from −100 to 100 °C, and the scanning rates were 10 °C/min. The resolution is ±0.2 μW.

*Index of Refraction.* An Abbe Refractometer from Bellingham and Stanley Limited, model 60/ED, was used to measure the index of refraction of the ionic liquid, with a water bath temperature control from Grant, model Y14, ± 0.1 °C.

*Spectroscopic Measurements.* UV/vis absorbance spectra were performed using a UV−vis−NIR Varian Cary 5000 spectrophotometer (spectral range from 300 to 800 nm). Luminescence spectra were measured using a SPEX Fluorolog-3 Model FL3-22 spectrofluorimeter, with 0.5 nm slits. Excitation wavelength was 360 nm, and experiments were performed at room temperature (22 °C). Lifetime measurements were run on a LKS.60 ns laser photolysis spectrometer from Applied Photophysics, with a Brilliant Q-Switch Nd:YAG laser from Quantel, using the second harmonic ($\lambda_{exc}$ = 355 nm, laser pulse half-width equal to 6 ns). Emission decays were obtained with spectral resolution of 2 nm, with a perpendicular geometry in relation with the laser excitation, by averaging between 2 to 10 measurements at each emission wavelength depending on the emission intensity of the sample. An optical cutoff filter (570 nm) for the emitted light was used to avoid scattering light contamination. Luminescence decay traces at each wavelength were analyzed using least-squares fittings of the experimental data, using Solver from Microsoft Excel. The measurements were done melting the ionic liquid and spreading it on the surface of a quartz glass triangular cuvette (thickness of about 0.5 mm). Temperature measurements were done with the cuvette filled with water. Temperature control was performed with a water bath connected to the spectrophotometer, with an approximate accuracy of ±1 °C.

## RESULTS AND DISCUSSION

**$[P_{6,6,6,14}][Eu(NTA)_4]$ as an Ionic Liquid.** *DSC Studies.* DSC measurements showed that the ionic liquid under study had an interesting behavior (Figure 1). The first cooling run, starting at room temperature and descending until −65 °C (not in the Figure), does not show any thermochemical process. Heating from −65 to 80 °C (curve a in Figure 1) a clear endothermic peak (that can be associated with the melting of the ionic liquid) is noted. However, the second cooling run from 80 °C to −65 °C still does not show thermochemical processes (curve b, Figure 1). The second heating (curve c, Figure 1) displays a exothermic peak around −4 °C and the endothermic peak around 63 °C observed in the first heating run. The first peak can be associated to a cold crystallization while the second one to the melting of the ionic liquid. In addition, a closer inspection detects a smaller bump near −50 °C that could be associated to a glass transition. The values obtained for the two melting points and the cold crystallization are compiled in Table 1. The possible glass transition is too small and too close to the starting temperature of the run to be quantifiable.

The most interesting feature is the possibility of having a metastable liquid when the ionic liquid is cooled. The fusion


dx.doi.org/10.1021/ic3023024 | Inorg. Chem. 2013, 52, 3755−3764

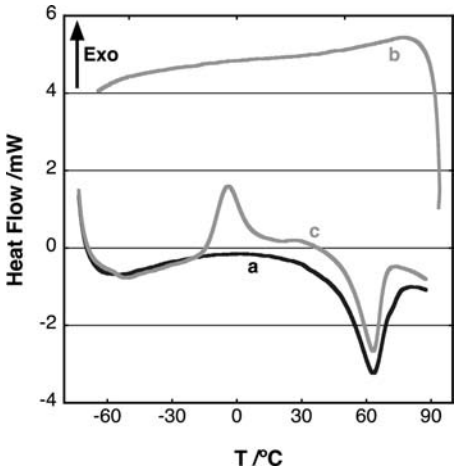


**Figure 1.** DSC measurements of $[P_{6,6,6,14}][Eu(NTA)_4]$; (a) first heating cycle, (b) second cooling cycle, (c) second heating cycle.

**Table 1. Data from DSC Runs**

| | onset point /°C | peak/°C | enthalpy/J $g^{-1}$ |
|---|---|---|---|
| fusion-first heating | 47.1 | 63.0 | 17.4 |
| fusion-second heating | 50.1 | 63.1 | 11.8 |
| cold crystallization | −14.2 | −4.0 | −10.2 |

enthalpies in the first and second heating cycles are not coincident, which can be caused by two different polymorphs fusing; in the first one the most stable at room temperature and in the second one the polymorph formed at −14 °C that does not have not enough time to relax to the initial one during the DSC run. This second polymorph would be around 5.6 J $g^{-1}$ less stable than the first one. Another very interesting point is the behavior in steady-state emission spectroscopy (Figure 9, see below). A change is clearly detected at the fusion temperature of the ionic liquid. These data are rather similar to results published very recently with lanthanide ionic liquids.[20,21]

*NMR Studies.* NMR data was collected for the compound $[P_{6,6,6,14}][Eu(NTA)_4]$ in its solid and molten forms, as well as dissolved in deuterated acetonitrile, benzene, and methanol. Additional samples of the compound placed in excess ionic-liquid phosphonium chloride $[P_{6,6,6,14}]Cl$ and of the intact ligand HNTA in similar solvents and media were used for comparison.

$^1H$ NMR resonances of the compound $[P_{6,6,6,14}][Eu(NTA)_4]$ dissolved in organic solvents appeared in two separate spectral windows: one (region of 4 to 0 ppm) containing the aliphatic resonances due to $[P_{6,6,6,14}]^+$ with a pattern which was, in all samples, similar to that appearing for pure $[P_{6,6,6,14}][Cl]$; and the other (region of 9 to 6 ppm) displaying the aromatic resonances of the $NTA^-$ moieties complexed to Eu(III). The ratio of the integrated intensities of the $^1H$ (aliphatic/aromatic) signals was approximately 2:1, as predicted, although in benzene the value was somewhat affected by putative resonances hiding under the solvent peak. In methanol, the $^1H$ NMR aromatic resonances in the aromatic region, the $^{13}C$-$^1H$ HSQC correlation signals and the $^{19}F$ signals all exhibited shifts and bandwidths very similar to those found for HNTA in the same solvent, with the notable exception of the C and H resonances due to the CH bridging the ketone groups, which are absent in the spectra of the compound. In benzene and acetonitrile, $^1H$ and $^{13}C$ aromatic signals were considerably broadened, albeit with no significant chemical shift variation. Also, in these solvents, the $^{19}F$ NMR spectra showed at least two new, very broad (100 to 200 Hz) resonances confirmed by EXSY experiments to be due to exchanging fluorine-containing species. These results may indicate that the Eu(III) complex is inherently unstable and/or extremely labile in methanol but that in benzene and acetonitrile there are at least two $[P_{6,6,6,14}][Eu(NTA)_4]$ stable conformers in slow to moderate exchange; this discouraged any attempt by us to correlate the broadening of resonances to the paramagnetic effect of the central Eu(III) ion. As previously reported,[22,23] $^{19}F$ NMR data obtained for a $-CF_3$ reporter group attached to the Ln(III) ligand can supply information about exchange phenomena affecting the Ln(III) complex.

As seen in DSC experiments, $[P_{6,6,6,14}][Eu(NTA)_4]$ changes from an opaque powdered solid to an optically transparent, viscous medium above the melting point. The only signal appearing in the solid sample shows that the single detectable MR signal is a very broad $^{19}F$ signal centered at −68 ppm with a bandwidth of about 3000 Hz. Upon raising the temperature to about 75 °C, this $^{19}F$ NMR signal splits in two the about 100 Hz bandwidth resonances, indicating an overall enhancement in the $-CF_3$ group mobility and the existence of at least two stable isomers with different $-CF_3$ positioning (see Figure 2).

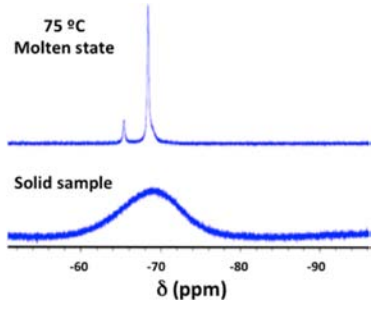


**Figure 2.** $^{19}F$ NMR signal of $[P_{6,6,6,14}][Eu(NTA)_4]$: solid sample and at 75 °C (liquid sample).

Very broad $^1H$ resonances also appear from 75 °C upward, with chemical shifts shifted about 10 ppm downfield to those observed in solution, which stabilize after several minutes when held at 90 °C. These features are maintained even when the temperature is lowered to 50 °C and, indeed, broad $^1H$ signals at low field are still observed when the sample remains at 25 °C for up to 2 h (see Figure 3). The resolidification is thus not symmetric to the fusion process, in accordance with DSC runs, displaying a strong hysteresis effect due to the formation of the supercooled ionic liquid.

**UV/vis Absorption Spectroscopy and Emission Spectroscopy Studies.** $[P_{6,6,6,14}][Eu(NTA)_4]$ absorption spectra were measured in its pure form and dissolved in toluene, cyclohexane, 1-butanol, propylene carbonate and methanol, some of them shown in Figure 4. As expected, the ligand absorption spectra completely dominates because the Eu(III) f-f electronic transitions are forbidden and have very low extinction coefficients. The ligand absorption spectra do not show significant solvatochromic effects. The larger difference is for the pure ionic liquid, where a redshift and band broadening is found. This result indicates aggregation of NTA in the ionic liquid form, probably forming dimers or even higher order


dx.doi.org/10.1021/ic3023024 | Inorg. Chem. 2013, 52, 3755−3764

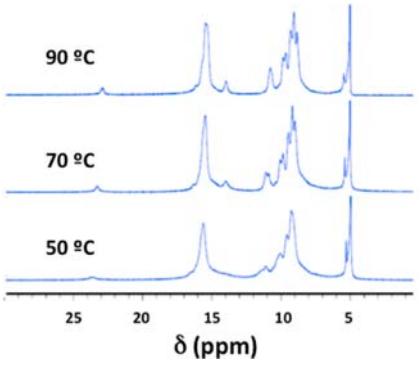


**Figure 3.** $^{1}$H NMR signal of $[P_{6,6,6,14}][Eu(NTA)_4]$: cooling effect from 90 to 50 °C.

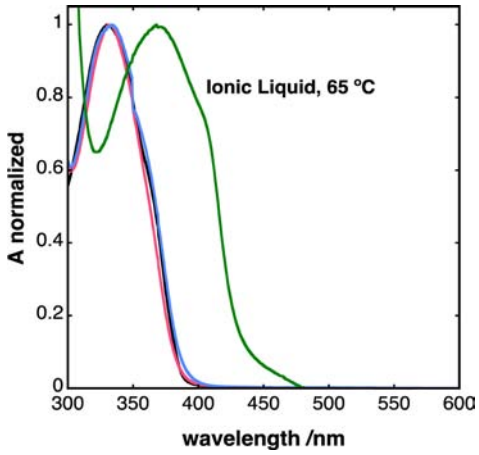


**Figure 4.** $[P_{6,6,6,14}][Eu(NTA)_4]$ absorption spectra (green, 65 °C) and dissolved in cyclohexane, methanol, and toluene (black, red, and blue, room temperature).

aggregates. As a result, the ionic liquid $[P_{6,6,6,14}][Eu(NTA)_4]$ is yellowish while in solution it is colorless.

$[P_{6,6,6,14}][Eu(NTA)_4]$ emission spectra has two components, one due to the ligand characterized by a broad and structure less emission band spanning from 400 nm to about 550 nm, and another due to Eu(III), characterized by sharp emission peaks around 600 nm (Figure 5). Because of the "antenna effect", Eu(III) dominates the emission spectra, and the

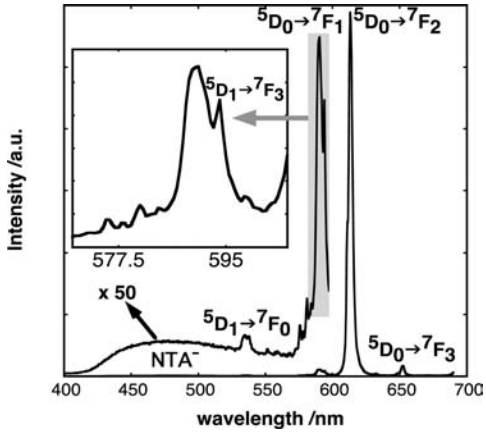


**Figure 5.** $[P_{6,6,6,14}][Eu(NTA)_4]$ emission spectra at 71 °C ($\lambda_{ex}$ = 360 nm).

luminescent glow is red whatever the state (in solution or by itself) of the compound is. The details of the typical Eu(III) emission spectra are rich and briefly described below (there are several reviews where the theory is described in detail, see, for example, reference 7).

The Eu(III) luminescence spectra are characterized by several peaks corresponding to electronic transitions from Eu(III) $^5D_0$ state to $^7F_J$ states ($J$ = 0, 1, ...6). $^5D_0$ and $^7F_0$ are nondegenerate states, that is, the presence of a crystal-field does not lead to a splitting of the energy of the Stark levels. Nevertheless, depending of the crystal field point group symmetry, the remaining $^7F_n$ states ($n$ = 1, ...6) have several Stark levels.[24,25] The most important case is the $^5D_0 \rightarrow {}^7F_1$ transition, which is forbidden in terms of electric dipole (ED) moment but is allowed in terms of magnetic dipole (MD) moment and therefore appears in the Eu(III) emission spectra. The intensity of this band is almost insensitive to the environment, being affected solely by the index of refraction.[26] This allows the use of this transition as an internal standard calibration for the other emission bands, and also gives important information about the crystal field point group symmetry, depending on the number of peaks present on its emission band. Since the $^5D_0$ state is always nondegenerate, the number of peaks gives direct information about the number of Stark levels of the $^7F_1$ state, and therefore the possible crystal field point group symmetry.[24]

Another important transition is $^5D_0 \rightarrow {}^7F_0$. Both states are always nondegenerate, and therefore only a single peak is expected. However this transition is forbidden under both mechanisms discussed above. The perturbation caused by the crystal-field leads to *J-J* mixing with the electric dipole allowed $^5D_0 \rightarrow {}^7F_2$ transition, and therefore the $^5D_0 \rightarrow {}^7F_0$ transition appears in the luminescence spectra with relatively low intensity as a single peak.[25,27] The same mechanism is also responsible for $^5D_0 \rightarrow {}^7F_3$ and $^5D_0 \rightarrow {}^7F_5$ transitions, although these are always weak. $^5D_0 \rightarrow {}^7F_2$, $^5D_0 \rightarrow {}^7F_4$, and $^5D_0 \rightarrow {}^7F_6$ transitions are all allowed through the ED mechanism and are highly sensitive to the environment, especially the $^5D_0 \rightarrow {}^7F_2$ emission peak, sometimes called the hypersensitive transition.

On the $[P_{6,6,6,14}][Eu(NTA)_4]$ emission spectrum, presented in Figure 5, the $^5D_0 \rightarrow {}^7F_1$ transition shows a single peak within the present wavelength resolution, although a small peak to the red is also detected. As seen above, the origin of this peak can be connected with the $^5D_1 \rightarrow {}^7F_3$ transition: since the excitation is at 360 nm, $^5D_1$ states are also generated. Nevertheless, steady-state luminescence intensity of other bands originated from $^5D_1$ states is rather low. The $^5D_0 \rightarrow {}^7F_0$ peak has a very low intensity that may well be within the background noise. This indicates a high symmetry group for the complex, but further assignment is prevented by the present spectral resolution.

The $^5D_0 \rightarrow {}^7F_2$ band intensity when compared with that of the $^5D_0 \rightarrow {}^7F_1$ transition also gives important information about the bond between the ligand and the complex. The ratio of intensities can be analyzed according to the Judd–Ofelt theory.[7,28] This theory is based on the model where the intensity of the forbidden f-f ED transitions appears from the admixture into the $4f^N$ configuration of configurations of opposite parity. The crystal field potential generated by point charges located at atom positions of the ligands appears in the theory as the perturbation for mixing states of different parity into the $4f^N$ configuration. In the Judd–Ofelt theory it is also considered that the Stark levels at the ground state are equally populated, an assumption reasonable for experiments at room


dx.doi.org/10.1021/ic3023024 | *Inorg. Chem.* 2013, 52, 3755–3764

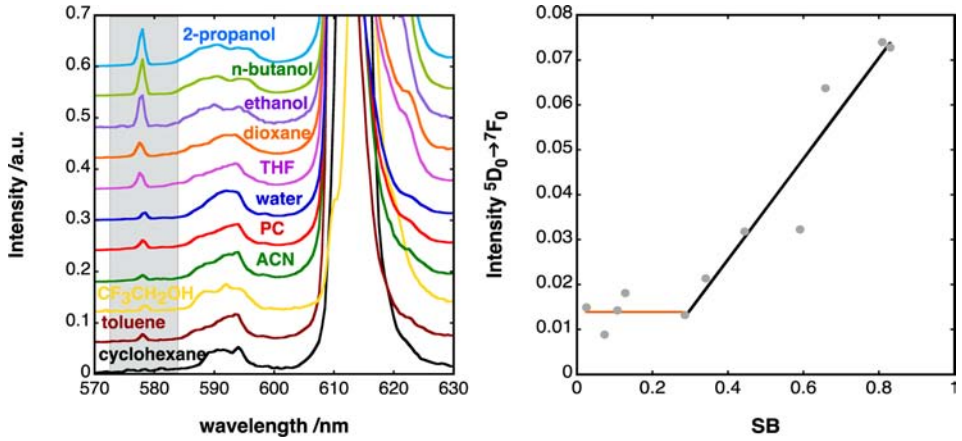


**Figure 6.** $[P_{6,6,6,14}][Eu(NTA)_4]$ in solution: emission spectra ($\lambda_{ex}$ = 360 nm, room temperature) and correlation of the $^5D_0 \rightarrow {}^7F_0$ emission line with the SB.

temperature, and with an optically isotropic host matrix. So only ED transitions between different manifolds are considered, which simplifies the problem.

Three phenomenological intensity parameters appear in this theory ($\Omega_\lambda$, with $\lambda$ = 2, 4, and 6), which are related with the dipole strength $D$ of the electronic transition through[7]

$$D = \frac{1}{(2J+1)} \frac{(n^2+2)^2}{9n} e^2 \sum_{\lambda=2,4,6} \Omega_\lambda \langle f^N \Psi J \| U^{(\lambda)} \| f^N \Psi' J' \rangle^2 \quad (1)$$

$\langle f^N \Psi J \| U^{(\lambda)} \| f^N \Psi' J' \rangle$ are reduced matrix elements and were previously calculated by Carnall et al.,[29] $e$ is the elementary charge, and $n$ is the medium index of refraction which should be taken into account since the lanthanide ion is in a dielectric medium and, therefore, affected by polarizability interactions with the host matrix. This is the framework to analyze Eu(III) spectra in which $\Omega_\lambda$ can be calculated. In the emission spectra, one can analyze results through the probability of an ED transition in lanthanides ($A_J$), given by:

$$A_J^{ED} = \frac{64\pi^4 e^2 \bar{\nu}^3}{3h(2J+1)} \frac{n(n^2+2)^2}{9} \sum_{\lambda=2,4,6} \Omega_\lambda \langle f^N \Psi J \| U^{(\lambda)} \| f^N \Psi' J' \rangle^2 \quad (2)$$

Now $A_J$ can be calculated through eq 2, provided $n$ and $\Omega_\lambda$ are known. In the case these values are unavailable, one can analyze individually each emission band. For Eu(III), it is known that the $^5D_0 \rightarrow {}^7F_1$ transition depends weakly on the environment and has a negligible ED mechanism, and therefore is fairly constant, and its $A_{J=1}$ can be taken from the literature assuming some reasonable value for the index of refraction.[26] The dependence of a magnetic dipole transition with the index of refraction is

$$A_J^{MD} = \frac{64\pi^4 e^2 \bar{\nu}^3}{3h(2J+1)} n^3 D_{MD} \quad (3)$$

with $D^{MD}_{J=1} = 9.4 \times 10^{-6}$ Debye.[2] One can therefore define the following relation:

$$\gamma_J = \frac{A_J^{ED}}{A_{J=1}^{MD}} \quad (4)$$

which is the intensity ratio between each transition and the $^5D_0 \rightarrow {}^7F_1$ band, a value that can be obtained from experimental data. Assuming $D^{MD}_{J=1}$ is taken from the literature, the remaining $A_J$ are obtained in a straightforward way and $\Omega_\lambda$ might be calculated (considering the MD mechanism negligible for the other transitions)

$$\Omega_\lambda = \frac{A_{J=\lambda}}{A_{J=1}} \frac{9n^2}{(n^2+2)^2} \left( \frac{\bar{\nu}_\lambda}{\bar{\nu}_{j=1}} \right)^3 \frac{D^{MD}_{J=1}}{\langle f^N \Psi J \| U^{(\lambda)} \| f^N \Psi' J' \rangle} \quad (5)$$

It is important to point out that $A_{J=\lambda}/A_{J=1}$ is an experimental value that can be calculated by the integral intensity ratio of each transition over the MD transition. Therefore, the only assumption is concerned with the index of refraction, but even $(9n^2)/(n^2+2)^2$ is approximately equal to 1 for indexes of refraction values until 2 (the error is about 10%) if this parameter is not available. From the emission spectra in Figure 1 and the experimentally determined index of refraction ($n$ = 1.641), an estimated value of $\Omega_2$ equal to $40.9 \times 10^{-20}$ cm$^2$ is obtained. The value of the $\Omega_2$ parameter gives an insight about the covalent character of the Eu(III)−NTA bond, being higher when the covalency character increases.[30] Typically the obtained value is in accordance to what is usually observed for Eu(III) complexes.[7]

**Solvent Effects in the $[P_{6,6,6,14}][Eu(NTA)_4]$ Luminescence Spectra.** Upon dissolution, all Eu(III) emission peaks show pronounced solvent effects. The $^5D_0 \rightarrow {}^7F_0$ peak appears in almost all solvents as depicted in Figure 6. This transition is not allowed, but in $C_s$, $C_n$, or $C_{nv}$ symmetry groups it appears because of the mechanism discussed above. So this is a direct indication that the symmetry group (and hence Eu(III) coordination) changes in solution. The $^5D_0 \rightarrow {}^7F_1$ peak also splits into 3 peaks, indicating a sharp decrease of symmetry.

The relative intensity of the $^5D_0 \rightarrow {}^7F_0$ peak was plotted vs several empirical solvent polarity scales to have an insight about the mechanism underlying the appearance of this peak. $E_T(30)$ is perhaps one of the most popular empirical polarity scales, giving information if the solvent polarity and proticity play a role.[31] In our case no correlation was observed. Other options include the solvent dielectric constant or the index of refraction, which also do not show any correlation. These results point out that the solvent polarity and hydrogen ability do not affect significantly the intensity of the $^5D_0 \rightarrow {}^7F_0$ peak. Therefore multiparametric polarity scales were explored. The Kamlet−Taft multiparametric polarity scale is the most well-known[32]


dx.doi.org/10.1021/ic3023024 | Inorg. Chem. 2013, 52, 3755−3764

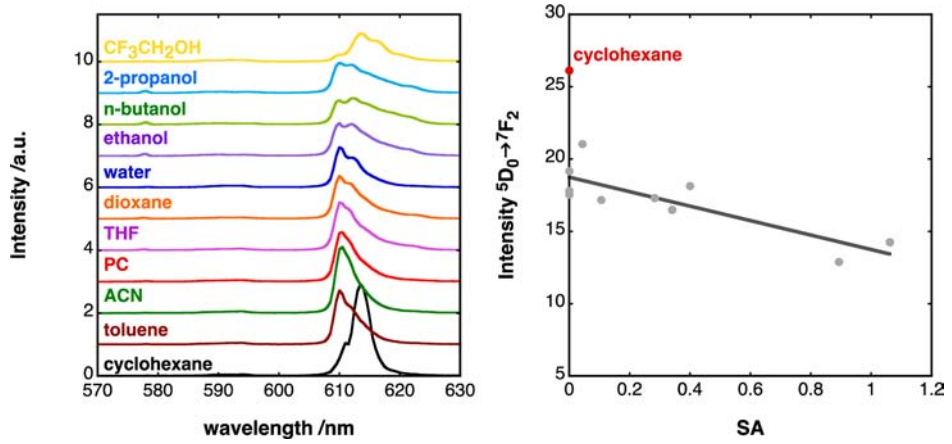


**Figure 7.** $[P_{6,6,6,14}][Eu(NTA)_4]$ in solution: emission spectra ($\lambda_{ex}$ = 360 nm, room temperature) and correlation of $^5D_0 \rightarrow {}^7F_2$ emission line with the SA.

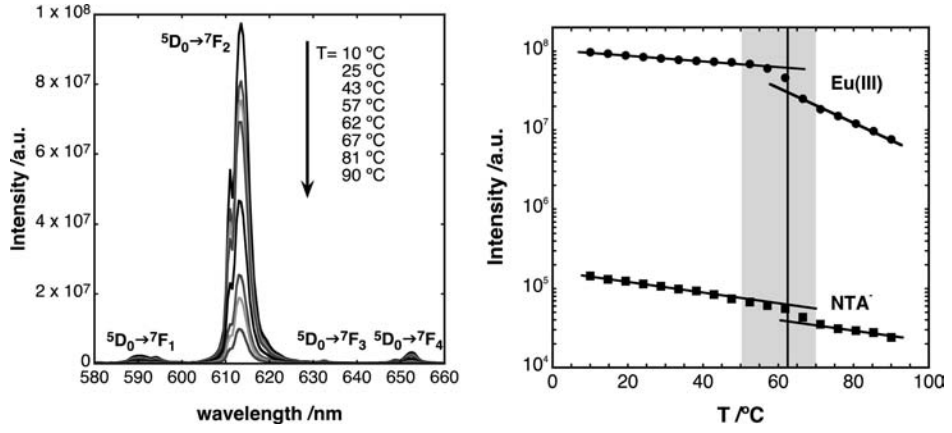


**Figure 8.** Temperature effects on the $[P_{6,6,6,14}][Eu(NTA)_4]$ emission spectra ($\lambda_{ex}$ = 360 nm, left) and dependence with temperature of the emission intensity intrinsic to Eu(III) luminescence ($\lambda_{em}$ = 614 nm) and $NTA^-$ luminescence ($\lambda_{em}$ = 470 nm, right).

$$XYZ = XYZ_0 + s\cdot\pi^* + a\cdot\alpha + b\cdot\beta + d\cdot\delta \quad (6)$$

where $\pi^*$ accounts for dipolar interactions, $\alpha$ is a solvent proticity scale, $\beta$ a basicity scale, and $\delta$ is a correction for polarizability effects. XYZ is the solute property under study and $XYZ_0$, $s$, $d$, $a$, and $b$ are solute intrinsic parameters accounting for the influence of each solvent property in the measurement. Later Cátalan proposed a new generalized polarity scale similar to that proposed by Kamlet–Taft,[33] but with a more detailed description of nonspecific solvent effects (dipolarity and polarizability). As in the other case, a solvent acidity (SA) and a solvent basicity (SB)[34] scale are proposed in which a correlation with $\alpha$ and $\beta$ is found. Both multiparametric approaches give similar conclusions, nevertheless the Cátalan scale gives rise to better correlations, which are shown below (see Figure 6 and 7). What can we learn from those plots? The $^5D_0 \rightarrow {}^7F_0$ peak intensity clearly increases with solvent basicity (Figure 6). This points to a labile coordination between europium and the solvent, which grows stronger as its basicity/nucleophilicity increases, changing the geometry of the complex.

For the $^5D_0 \rightarrow {}^7F_2$ peak intensity, the main correlation is with the solvent acidity (see Figure 7). Therefore this points to a decrease of covalency of the bond between NTA and Eu(III). The cyclohexane red point, however, is out of the correlation, which may be due to ion pairs that prevent this solvent from interacting with Eu(III).

These results point out two different solvent effects: basicity enhances the coordination of solvent molecules with Eu(III), while acidity/proticity gives rise to interactions between the solvent molecules and NTA. So while aprotic solvents (such as cyclohexane or toluene) are relatively innocuous for the complex stability, with other solvents such as alcohols the stability is compromised (usually the complex decomposed within 1 day). Some solvents like water and trifluoroethanol have low basicity (hence low coordination character with Eu(III)), but their proticity leads to strong interactions with NTA that will also compromise its stability. These results are also in accordance with NMR data, where the instability of the compound dissolved in methanol is highlighted. The presence of two stable conformations in solvents such as benzene and acetonitrile are not completely evident, but indeed a significant change of the $^5D_0 \rightarrow {}^7F_2$ peak intensity is seen from cyclohexane to solvents such as toluene.

**Temperature Effects in $[P_{6,6,6,14}][Eu(NTA)_4]$ Luminescence.** *Steady-State Emission Spectroscopy.* Figure 8 shows the temperature dependence of ionic liquid $[P_{6,6,6,14}][Eu(NTA)_4]$ emission spectra. Its intensity has a small variation below the melting point in the solid state. However between 55 and 62 °C the intensity sharply decreases without changing significantly the emission band shape. This temperature range is coincident with the melting process observed above on both DSC and NMR measurements. Therefore the compound in the


dx.doi.org/10.1021/ic3023024 | Inorg. Chem. 2013, 52, 3755–3764

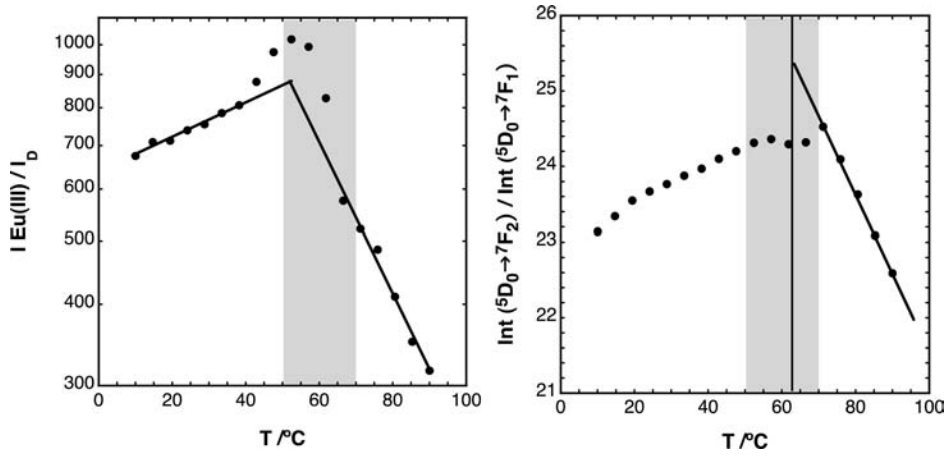


**Figure 9.** Dependence with temperature of the ratio of intensity due to Eu(III) ($\lambda_{em}$ = 614 nm) and NTA$^-$ ($\lambda_{em}$ = 470 nm), left, and of the ratio between $^5D_0 \rightarrow {}^7F_2$ and $^5D_0 \rightarrow {}^7F_1$ Eu(III) emission bands, right.

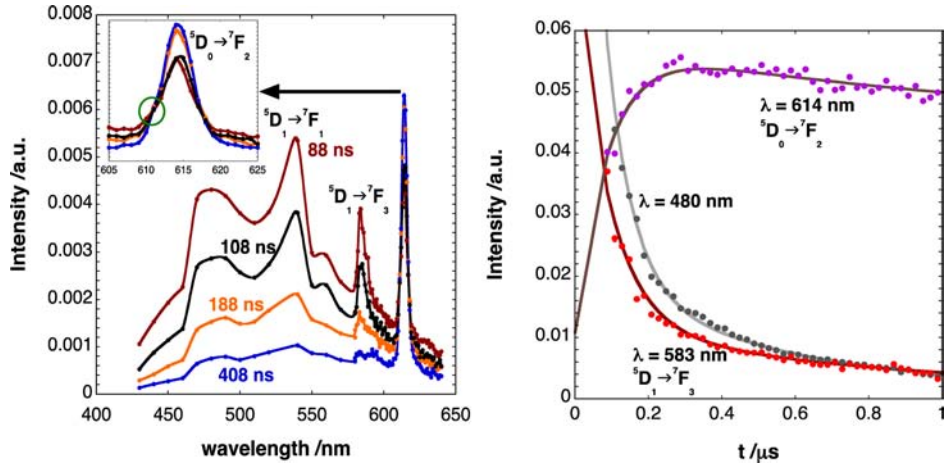


**Figure 10.** Time-resolved emission spectra at several time delays, left, and luminescence decays in the submicrosecond time scale at 480, 583, and 614 nm, right. Solid lines are fits with exponential functions with a kinetc time of about 100 ns.

liquid state has lower luminescence intensity, as expected for a less "rigid" environment. In the liquid state, a larger variation with temperature is observed as well. The same effect is also seen on the low intensity ligand band.

The antenna effect can be probed by calculating the emission intensity ratio between the lanthanide and the ligand, as shown in Figure 9. Below the melting point, this efficiency increases with temperature indicating a higher coupling effect. In the melting point region, a departure from Arrhenius like behavior is observed with a maximum coinciding with the melting point. However, in the liquid phase, it starts to decrease steeply with temperature probably because the less "rigid" environment prevents a strong coupling between donor and acceptor. Also the ratio of intensities between the Eu(III) $^5D_0 \rightarrow {}^7F_2$ and $^5D_0 \rightarrow {}^7F_1$ emission peaks, which are proportional to $\Omega_2$, have a change of behavior in the melting point region. From those results one can conclude that the covalency of the bond is temperature dependent especially in the liquid phase region as correlated by Arrhenius type behavior.

It is noteworthy to point out that the strong variations around the melting point seen here are not that usual. Kocher et al.[35] have studied an ionic liquid crystal containing 5% (w/w) europium nitrate as a dopant, and while the transition from crystal to liquid crystal was seen from Eu(III) photoluminescence provided it was not a glassy transition (as pointed out by Suarez et al.[36]), other phase transitions from crystal to smectic A phase and from smectic A phase to isotropic liquid are not seen from luminescence measurements. Taking into account those previous reports, the transitions seen here probably are due to crystalline phases melting at around 65 °C, giving rise to the effects shown on Figures 8 and 9. Also in this case the ligand is excited but not the lanthanide, and therefore other effects such temperature dependent aggregation should play an important role.

*Time-Resolved Luminescence.* Time-resolved emission spectra at 67 °C (above the melting point) are shown in Figure 10. In the submicrosecond time scale, the emission spectra are dominated by the ligand. Within about 400 ns this emission vanishes, giving rise at the same time to the sharp Eu(III) emission peaks. The kinetics of this process is rather independent of temperature. At the same time, emission coming from the Eu(III) $^5D_1$ state is also detected. Since Eu(III) is not directly excited, one would expect a rise time for the emission intensity coming from this state. This, however, is not experimentally observed, and therefore this state should be populated at a much shorter time scale possibly from the ligand singlet excited-state. This configures a situation where energy-transfer to Eu(III) is rather efficient, and of course it also explains why we almost do not see the ligand in the steady-state emission spectra. The emission decays show a kinetics similar


dx.doi.org/10.1021/ic3023024 | Inorg. Chem. 2013, 52, 3755−3764

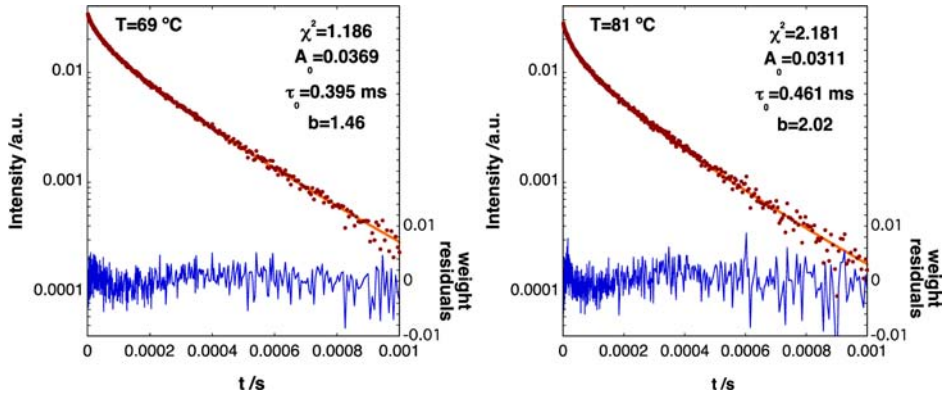


**Figure 11.** Eu(III) luminescence decays at two different temperatures. Fittings were done with eq 7.

for both ligand and the Eu(III) $^5D_1$ state, with a concomitant rise time of the Eu(III) $^5D_0$ state.

The $^5D_0 \rightarrow {}^7F_2$ emission decay is nonexponential, see Figure 11. The shape of the luminescence decays has clearly a transient followed by an exponential tail. These results could be explained using the following equation[37]

$$I_{Eu(III)} = A_0 \exp\left[-\left(\frac{t}{\tau_0} + b\sqrt{\frac{t}{\tau_0}}\right)\right] \quad (7)$$

where $\tau_0$ is the Eu(III) decay time and $b$ is here an experimental value determined from the fitting. Table 2 summarizes the results obtained for the ionic liquid (i.e., above the melting point).

**Table 2. Results of the Fitting of Eu(III) Luminescence Decays with Equation 7**

| $T$ (°C) | $A_0$ (±0.03) | $\tau_0$ (ms; ± 0.02 ms) | $b$ (±0.1) | $\chi^2$ |
|---|---|---|---|---|
| 67.2 | 1.00 | 0.39 | 1.4 | 1.71 |
| 69.0 | 1.16 | 0.40 | 1.5 | 1.19 |
| 70.2 | 1.14 | 0.41 | 1.5 | 1.56 |
| 70.6 | 1.21 | 0.42 | 1.6 | 1.61 |
| 71.6 | 1.17 | 0.42 | 1.6 | 1.49 |
| 72.7 | 1.11 | 0.42 | 1.6 | 1.37 |
| 73.8 | 1.13 | 0.42 | 1.7 | 1.76 |
| 75.1 | 1.13 | 0.43 | 1.8 | 1.55 |
| 75.9 | 1.10 | 0.42 | 1.7 | 1.77 |
| 76.8 | 1.08 | 0.44 | 1.8 | 1.74 |
| 78.4 | 1.05 | 0.44 | 1.9 | 1.88 |
| 79.2 | 1.03 | 0.44 | 1.9 | 1.95 |
| 80.1 | 1.02 | 0.45 | 2.0 | 1.89 |
| 81.3 | 0.98 | 0.46 | 2.0 | 2.18 |

This equation is particularly useful for temperatures close to the melting point, but the quality of the fitting gradually decreases with temperature. The luminescence spectral shape does not change over this time-range, indicating that the light emitters are always equivalent. One possible explanation is a self-quenching effect between $[Eu(NTA)_4]$ complexes. Such quenching can be either due to an electron or an energy-transfer mechanism between an excited-state and a ground-state complex. The case for a electron-transfer mechanism does not seem likely, since the $^5D_0$ state of Eu(III) has its excited-state electron in an f orbital, shielded from the surroundings by other atomic orbitals. The case for Förster energy-transfer mechanism is, therefore, more likely. Since there is no overlap between NTA absorption spectra and Eu(III) emission spectra, such mechanism must proceed via energy-transfer between Eu(III) (an homoatomic energy-transfer process). In such case, eq 7 is explained when the material is basically "frozen", and the transient process arises from the random distribution of distances (and orientations) between donor and acceptor molecules.[37] In such case it follows that for assemblies of homologue chromophores:

$$b = \sqrt{\frac{\pi}{2}}\, C \frac{4}{3}\pi R_0^3 \quad (8)$$

where $C$ is the chromophore concentration (number of molecules/Å$^3$) (in this case, ground-state complexes) and $R_0$ is the Förster critical distance (in Å). Therefore, this parameter should be proportional to the concentration of complexes, which in this case should be proportional to density. Interestingly, this parameter increases with temperature, see Figure 12, leading to a naive conclusion that the ionic liquid density would increase with temperature. This does not seem plausible: a more sensible conclusion is that the diffusional contribution for the transient increases with temperature, leading to the increment of $b$. Nevertheless, it is important to note that the index of refraction was also measured as a function of temperature at this range (see Supporting Information) and that seems to point to a similar conclusion.

Concerning the Eu(III) excited-state lifetime, it follows that the radiative lifetime may be calculated from experimental values taken from the steady-state emission spectra using:[38]

$$\tau_r = \frac{1}{\sum_{J=0}^{6} A_J} \quad (9)$$

Figure 12 shows these values computed for different index of refraction values. It follows that these values are in good agreement, slightly higher which is typical of systems with a luminescence quantum yield below 1. However it is not feasible to determine any trend of nonradiative rate constants since the application of the model is questionable for higher temperatures. At temperatures close to the melting point, the luminescence quantum yield should be around 70%.

## CONCLUSIONS

$[P_{6,6,6,14}][Eu(NTA)_4]$ was synthesized and exhibits a melting point equal to 63 °C, and therefore it is classified as an ionic liquid. Its thermochemical properties are, however, complex, and a metastable liquid state may be achieved at lower temperatures. The complex shows Eu(III) photoluminescence


dx.doi.org/10.1021/ic3023024 | Inorg. Chem. 2013, 52, 3755−3764

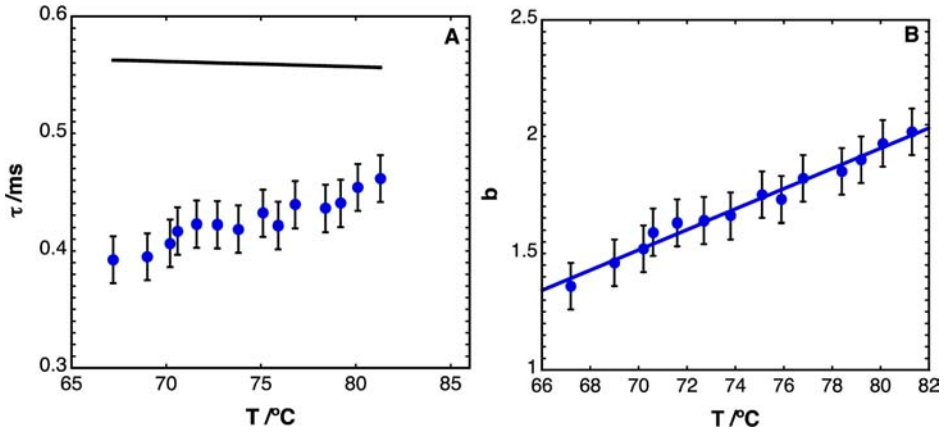


**Figure 12.** Temperature dependence of the results obtained from the fitting of Eu(III) luminescence decays with eq 7. Panel A shows the line corresponding to the values of Eu(III) radiative lifetime obtained from eq 9 using experimental index of refraction values.

which is enhanced by the antenna effect, through energy transfer from the ligand to the lanthanide, also seen in the submicrosecond time scale time-resolved emission spectroscopy. The Eu(III) emission spectra is in accordance with a high symmetry point group, as expected from the proposed structure. This, however, breaks down when the compound is dissolved in polar solvents such as *n*-alcohols, as seen from photoluminescence and NMR measurements. The transition from solid to liquid is evident from the photoluminescence temperature effects; while in the solid the temperature effects are minor, in the melting region and at higher temperatures the intensity changes strongly with temperature. Eu(III) luminescence decays in the submillisecond time scale point to excitation energy migration within the liquid. This result may be of importance for the future design of light-emitting devices using this type of material, which merits future research.

## ■ ASSOCIATED CONTENT

### Supporting Information

Further details on ESI and $^1$H NMR spectra are given in Figures S1−S3. This material is available free of charge via the Internet at http://pubs.acs.org.

## ■ AUTHOR INFORMATION

### Corresponding Author

*E-mail: claudia.pereira@itn.pt (C.C.L.P.), catl@fct.unl.pt (C.A.T.L.).

### Notes

The authors declare no competing financial interest.

## ■ ACKNOWLEDGMENTS

This work has been supported by Fundação para a Ciência e a Tecnologia through Grant no. PEst-C/EQB/LA0006/2011. Financial support from Fundação para a Ciência e a Tecnologia (FCT-MCTES) (projects PTDC/CTM/103664/2008, PTDC/QUI-QUI/114236/2009, and PTDC/CTM-NAN/120658/2010). The Restoration and Conservation Department at Faculdade de Ciências e Tecnologia is acknowledged for the FTIR Spectroscopy equipment used. This work was supported by Fundação para a Ciência e Tecnologia (FCT) under the "Ciência 2007" Programme. The NMR spectrometers are part of the National NMR Network (RNMN) and are funded by Fundação para a Ciência e Tecnologia.

## ■ REFERENCES

(1) Bruno, S. M.; Ferreira, R. A. S.; Carlos, L. D.; Pillinger, M.; Ribeiro-Claro, P.; Gonçalves, I. S. *Microporous Mesoporous Mater.* **2008**, *113*, 453−462.
(2) Bruno, S. M.; Ferreira, R. A. S.; Almeida Paz, F. A.; Carlos, L. D.; Pillinger, M.; Ribeiro-Claro, P.; Gonçalves, I. S. *Inorg. Chem.* **2009**, *48*, 4882−4895.
(3) Yokoyama, H. *Science* **1992**, *256*, 66−70.
(4) (a) Richardson, F. S. *Chem. Rev.* **1982**, *82*, 541. (b) Buonocore, G. E.; Li, H.; Marciniak, B. *Coord. Chem. Rev.* **1990**, *99*, 55−87.
(5) Zhang, W.; Xie, P.; Yin, M.; Chen, H.; Jing, L.; Zhang, Y.; Lou, L.; Xia, S. *J. Colloid Interface Sci.* **2003**, *262*, 588−593.
(6) Kido, J.; Okamoto, Y. *Chem. Rev.* **2002**, *102*, 2357−2368.
(7) Binnemans, K. Rare-Earth Beta-Diketonates. In *Handbook on the Physics and Chemistry of Rare Earths*; Gschneidner, K. A., Bunzli, J.-C. G., Pecharsky, V. K., Eds.; Elsevier: Amsterdam, The Netherlands, 2005; Vol. *35*, Chapter 225, p 107.
(8) Binnemans, K. *Chem. Rev.* **2009**, *109*, 4283−4374.
(9) Binnemans, K. *Chem. Rev.* **2007**, *107*, 2592−2614.
(10) Eliseeva, S. V.; Bünzli, J.-C. G. *Chem. Soc. Rev.* **2010**, *39*, 189−227.
(11) Biju, S.; Raj, D. B. A; Reddy, M. L. P.; Kariuki, B. M. *Inorg. Chem.* **2006**, *45*, 10651−10660.
(12) Mech, A.; Karbowiak, M.; Gorller-Walrand, C.; Van Deunc, R. *J. Alloys Compd.* **2008**, *451*, 215−219.
(13) Mudring, A.-V.; Tang, S.-F. *Eur. J. Inorg. Chem.* **2010**, 2569−2581.
(14) Tang, S.-F.; Mudring, A.-V. *Eur. J. Inorg. Chem.* **2009**, 2769−2775.
(15) Nockemann, P.; Beurer, E.; Driesen, K.; Van Deun, R.; Van Hecke, K.; Van Meervelt, L.; Binnemans, K. *Chem. Commun.* **2005**, *34*, 4354−4356.
(16) Lunstroot, K.; Driesen, K.; Nockemann, P.; Görller-Walrand, C.; Binnemans, K.; Bellayer, S.; Le Bideau, J.; Vioux, A. *Chem. Mater.* **2006**, *18*, 5711.
(17) Lunstroot, K.; Nockemann, P.; Van Hecke, K.; Van Meervelt, L.; Görller-Walrand, C.; Binnemans, K.; Driesen, K. *Inorg. Chem.* **2009**, *48*, 3018.
(18) Lunstroot, K.; Driesen, K.; Nockemann, P.; Van Hecke, K.; Van Meervelt, L.; Görller-Walrand, C.; Binnemans, K.; Bellayer, S.; Viau, L.; Le Bideau, J.; Vioux, A. *Dalton Trans.* **2009**, *2*, 298.
(19) Mehdi, H.; Binnemans, K.; Van Hecke, K.; Van Meervelt, L.; Nockemann, P. *Chem. Commun.* **2010**, *46*, 234−236.
(20) Chesman, A. S. R.; Yang, M.; Mallick, B.; Ross, T. M.; Gass, I. A.; Deacon, G. B.; Batten, S. R.; Mudring, A.-V. *Chem. Commun.* **2012**, *48*, 124−126.
(21) Chesman, A. S. R.; Yang, M.; Spiccia, N. D.; Deacon, G. B.; Batten, S. R.; Mudring, A.-V. *Chem.—Eur. J.* **2012**, *18*, 9580−9589.

(22) Kenwright, A. M.; Kuprov, I.; DeLuca, E.; Parker, D. *Chem. Commun.* **2008**, 2514−2516.
(23) Senanayake, P. K.; Kenwright, A. M.; Parker, D.; van der Hoorn, S. K. *Chem. Commun.* **2007**, 2923−2925.
(24) (a) Binnemans, K.; Gorller-Walrand, C. *J. Rare Earths* **1996**, *14*, 173−180. (b) Binnemans, K. *Bull. Soc. Chim. Belg.* **1996**, *105*, 793−798.
(25) Carlos, L. D.; Videira, A. L. L. *Phys. Rev. B* **1994**, *49*, 11721−11728.
(26) Gorller-Walrand, C.; Fluyt, L.; Ceulemans, A.; Carnall, W. T. *J. Chem. Phys.* **1991**, *95*, 3099−3106.
(27) Tanaka, M.; Nishimura, G.; Kushuda, T. *Phys. Rev. B* **1994**, *49*, 16917−16925.
(28) (a) Judd, B. R. *Phys. Rev.* **1962**, *127*, 750−761. (b) Ofelt, G. S. *J. Chem. Phys.* **1962**, *37*, 511−520.
(29) Carnall, W. T.; Fields, P. R.; Rajnak, K. *J. Chem. Phys.* **1968**, *49*, 4450−4455.
(30) Jørgensen, C. K.; Reisfeld, R. *J. Less-Common Met.* **1983**, *93*, 107−112.
(31) Reichardt, C. *Chem. Rev.* **1994**, *94*, 2319−2358.
(32) (a) Kamlet, M. J.; Abboud, J.-L. M.; Abraham, M. H.; Taft, R. W. *J. Org. Chem.* **1983**, *48*, 2877−2887. (b) Marcus, Y. *Chem. Soc. Rev.* **1993**, *22*, 409−416.
(33) Catalan, J.; Garcia de Paz, J. L.; Reichardt, C. *J. Phys. Chem. A* **2010**, *114*, 6226−6234.
(34) Catalan, J. *J. Phys. Chem. B* **2009**, *113*, 5951−5960.
(35) Kocher, J.; Gumy, F.; Chauvin, A.-S.; Bunzli, J.-C. G. *J. Mater. Chem.* **2007**, *17*, 654.
(36) Suárez, S.; Imbert, D.; Gumy, F.; Piguet, C.; Bunzli, J.-C. G. *Chem. Mater.* **2004**, *16*, 3257.
(37) Valeur, B. *Molecular Fluorescence: Principles and Applications*; Wiley-VCH: Weinheim, Germany, 2001.
(38) Ventura, M. G.; Laia, C. A. T.; Parola, A. J. *J. Phys. Chem. C* **2010**, *114*, 18414−18422.